

# SvfEye: A Semantic–Visual Fusion Framework with Multi-Scale Visual Context for Multimodal Reasoning

Yuxiang Shen<sup>a,b,1</sup>, Hailong Huang<sup>c,\*\*,1</sup>, Zhenkun Gao<sup>d,1</sup>, Xueheng Li<sup>a,b</sup>, Man Zhou<sup>a</sup>, Chengjun Xie<sup>b</sup>, haoxuan che<sup>e</sup>, Xuanhua He<sup>e,\*</sup> and Jie Zhang<sup>b,\*</sup>

<sup>a</sup>University of Science and Technology of China, Hefei, 230026, China

<sup>b</sup>Hefei Institutes of Physical Science, Chinese Academy of Sciences, Hefei, 230031, China

<sup>c</sup>Zhejiang University, Hangzhou, 310027, China

<sup>d</sup>East China Normal University, Shanghai, 200241, China

<sup>e</sup>The Hong Kong University of Science and Technology, Hong Kong, China

## ARTICLE INFO

### Keywords:

Training-free inference  
Fine-grained visual reasoning  
global-local visual context fusion  
semantic-visual fusion

## ABSTRACT

Multimodal Large Language Models (MLLMs) often struggle to accurately perceive fine-grained visual details, particularly in scenarios involving tiny or visually subtle targets. This challenge can be addressed through semantic–visual information fusion, which integrates global image context with fine-grained local evidence to achieve effective multi-scale visual understanding. Recently, a new paradigm termed “Thinking with Images” has emerged, enabling models to actively acquire high-resolution visual evidence by zooming or cropping image regions and fusing these local details with global context during reasoning. Although training-based approaches have demonstrated the effectiveness of this capability, they typically require extensive computational resources and large-scale task-specific data. Consequently, lightweight training-free methods have been proposed as a practical alternative to incorporate local visual evidence during inference. However, existing training-free approaches still suffer from two critical limitations during the fusion process. First, they indiscriminately extract and fuse local visual regions for all input instances regardless of actual necessity, introducing computational redundancy and perceptual noise. Second, they exhibit a drift between semantic intent and visual attention, which prevents accurate localization of user-focused regions. To address these challenges, we propose SvfEye, a novel training-free framework for adaptive visual–semantic fusion. SvfEye follows a two-stage pipeline: a Confidence-based Decision module determines whether additional local visual information is needed for a given instance, and a Semantic-attention Fusion module identifies where to extract informative local regions. This design enables the fusion of adaptive global-local visual information without additional training. Experiments show that SvfEye achieves substantial performance gains while obtaining an approximately 4.0× inference speedup over the state-of-the-art method ZoomEye, demonstrating the effectiveness of adaptive semantic–visual fusion for efficient multi-scale perception in MLLMs. Our code is publicly available at [github.com/Xiaoxiang100/SvfEye-final](https://github.com/Xiaoxiang100/SvfEye-final).

## 1. Introduction

In recent years, Multi-modal Large Language Models (MLLMs) [1, 25, 8, 3] have made significant progress in visual-language understanding [6, 11, 23]. The prevailing paradigm, “Thinking about Images,” [12] encodes images into static visual tokens and applies language-based reasoning mechanisms such as Chain-of-Thought [26]. However, this paradigm relies on a single-pass visual encoding process in which images are uniformly resized or cropped to fixed resolutions before reasoning. As a result, the model cannot selectively acquire high-resolution visual evidence when fine-grained details are required, leading to performance degradation on tasks involving tiny targets or subtle visual cues [14]. To address this limitation, a new paradigm termed “Thinking with Images” [19] has emerged, which equips

models with active perception capabilities for acquiring additional visual evidence during reasoning. Instead of relying solely on static visual representations, models can dynamically zoom, crop, or scan image regions to obtain informative local observations and integrate them with the global visual context. Such fusion of global context and local visual evidence enables the model to better capture fine-grained visual details that are difficult to perceive from a single-pass image encoding. This capability has been demonstrated by several training-based approaches such as DeepEyes [33] and V-Star [7]. However, these training-based approaches require extensive computational resources and task-specific data, motivating the exploration of training-free alternatives [9, 10] that enable dynamic fusion of global context and local visual evidence at inference time.

Recent training-free methods attempt to address this challenge through inference-time cost strategies. Existing methods typically fuse local visual context indiscriminately. To capture fine-grained visual details, these approaches fall into two categories. Search-based methods (e.g., DC<sup>2</sup> [24] and ZoomEye [21]), which iteratively evaluate regions but incur 5–10× inference overhead, and single-pass methods

\*Corresponding author

\*\*Project leader

ORCID(s): 0000-0003-2872-605X (M. Zhou); 0009-0004-6637-853X (X.

He); 0000-0002-0853-4379 (J. Zhang)

<sup>1</sup>Equal contribution

<sup>2</sup>This work was supported by the Anhui Provincial Natural Science Foundation, Grant No. 2408085MD090.

(e.g., MLLMs-Know [31]), which rely on attention maps for efficient localization but often struggle with fine-grained tasks. These methods reflect two fundamental challenges: (1) determining *when* local visual fusion is necessary, as current methods indiscriminately extract and fuse local visual sources for all input instances regardless of actual need; (2) identifying *where* to precisely localize targets by fusing explicit target semantics with visual attention, which effectively prevents spatial drift in fine-grained multi-object scenarios. Together, these questions of when to fuse and where to fuse constitute the core challenges of training-free visual-semantic fusion.

To validate these hypotheses and understand the underlying mechanisms, we conducted controlled experiments across multiple benchmarks, revealing two critical patterns (as shown in Sec 3.1).

**Observation 1: Models know *when* to fuse, but current methods don't ask.** Existing methods uniformly extract and fuse all local inputs under the assumption that finer details are always beneficial. However, our analysis shows that forced fusion degrades performance in some cases, as it often fails to add useful information for simple tasks and may instead introduce noise, as shown in Figure 3. Additionally, we observe systematic differences in the model's confidence distributions across tasks of varying difficulty, indicating that models inherently "know" when more local information is needed, yet existing methods fail to leverage this signal. This motivates our confidence-based decision module for determining when multi-scale visual context fusion is necessary. Importantly, unlike explicit prompting approaches that require extra generation steps, relying on internal token confidence is computationally free and significantly reduces overall inference latency. Nevertheless, even when local visual context is beneficial, current approaches still struggle with the challenge of precisely localizing targets.

**Observation 2: Attention-based methods struggle with handling multi-object problems.** While attention-based methods are efficient, they struggle with precise localization in multi-object scenarios. Attention maps highlight semantically relevant regions but often fail in multi-object settings, such as highlighting only a single target or deviating from the intended regions. Figure 5 reveals that raw attention mechanisms capture "what is relevant" rather than accurately resolving "where each object is". This motivates our semantic-attention Fusion module, which explicitly separates language intent from visual attention and uses semantic-visual fusion to determine *where* targets should be accurately aligned. These findings expose a fundamental gap: existing methods treat visual enhancement as uniform, whereas effective reasoning requires adaptive decisions about both whether additional visual fusion is needed and where to precisely localize relevant regions.

Building on these insights, we propose SvfEye, a training-free framework that addresses both dimensions of visual-semantic fusion. Unlike prior methods that force uniform fusion on all inputs, SvfEye dynamically determines *when* multi-scale visual context fusion is beneficial and *where* to

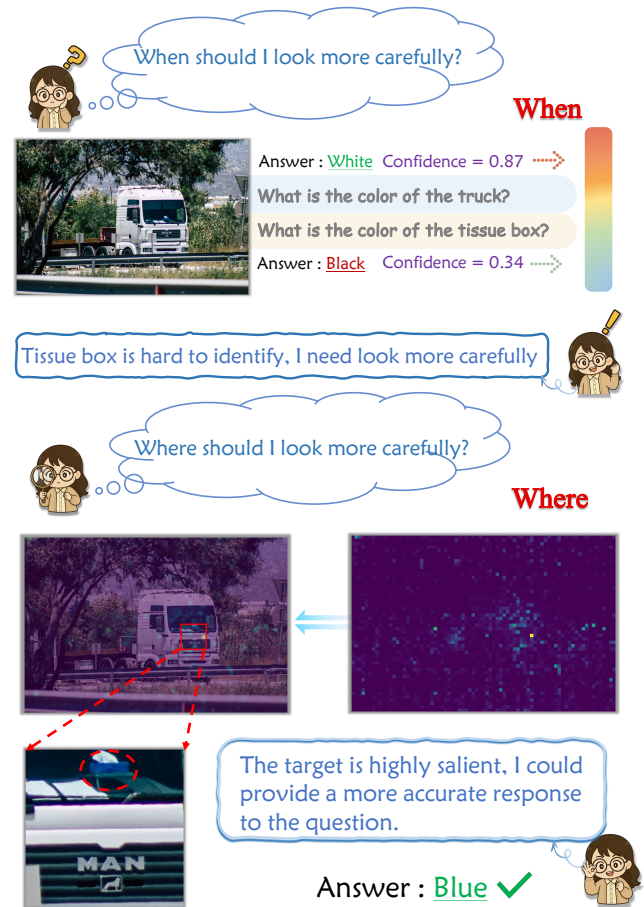


**Figure 1:** Illustration of SvfEye: Enabling MLLMs to dynamically decide whether and where to fuse local details.

precisely localize targets. For the *when* decision, SvfEye exploits intrinsic model confidence as a measure of information sufficiency, avoiding unnecessary and potentially noisy fusion when confidence is high. For the *where* decision, we introduce a semantic-attention fusion module that fuses decoupled semantic relevance with spatial positioning, enabling accurate target extraction in complex scenes. By integrating these modules, SvfEye achieves superior performance without iterative search overhead, consistently outperforming existing training-free methods with a 4.0× speedup across multiple benchmarks and effectively generalizing across diverse MLLMs.

Our contributions can be summarized as follows: (1) We identify two critical deficiencies in existing training-free methods through systematic empirical analysis: indiscriminate fusion of local details that degrades performance, and raw attention-based localization that suffers from spatial drift. (2) We propose **SvfEye**, a training-free framework enabling adaptive visual-semantic fusion by determining *when* and *where* to extract local sources through confidence-based decision and semantic-attention fusion. (3) Extensive experiments demonstrate that SvfEye achieves superior accuracy across multiple benchmarks while delivering a 4.0×

speedup, generalizing effectively across diverse MLLMs architectures.

## 2. Related Work

### 2.1. Multimodal Large Language Models

Multimodal Large Language Models (MLLMs) have made significant progress by aligning visual perception with textual reasoning. In modern architectures, a pre-trained vision encoder is connected to a frozen large language model via learnable fusion modules. These modules range from simple linear projections [17, 34] to query-based networks like Q-Formers [4], which map visual features into the semantic space of the LLM.

However, traditional MLLMs typically encode images at a fixed, low resolution, leading to the loss of fine-grained details. This limits their performance on tasks involving small objects or complex scenes [15, 27]. To preserve more visual information, recent models such as LLaVA-NeXT [16] and InternVL [2] adopt dynamic high-resolution strategies. They divide a high-resolution image into smaller patches, encode each patch independently, and directly concatenate the resulting visual tokens.

While these grid-based methods improve image clarity, they process all image patches uniformly. The LLM has to process all generated visual tokens, regardless of whether a patch contains useful targets or just empty background. This uniform processing naturally introduces unnecessary computational overhead and background noise. Therefore, an adaptive fusion approach is needed to selectively extract and integrate high-resolution visual details only from regions relevant to the current task.

### 2.2. Vision-Language Reasoning

To overcome the limitations of fixed-resolution processing, recent research enables MLLMs to actively interact with visual content, similar to how human eyes focus on specific regions. Current approaches to this active perception generally fall into two categories: training-based and training-free methods.

Training-based approaches, such as DeepEyes [33] and Pixel Reasoner [22], teach models how to crop and zoom through reinforcement learning or supervised step-by-step visual trajectories. While effective, these methods are highly expensive. They require massive amounts of specialized training data and computational resources. Moreover, the learned perception strategies are tightly bound to the specific model during training, making it difficult to apply them to other off-the-shelf MLLMs.

To avoid these high training costs, training-free methods attempt to simulate human-like zooming directly during the inference stage. Early training-free methods rely on iterative search. For example, ZoomEye [21] crops images into smaller patches and explores them through a hierarchical tree. Although this search-based approach finds fine-grained details accurately, the multi-round evaluation process is extremely slow, resulting in high inference latency. More efficient approaches, such as ViCrop [31], use internal

cross-attention maps to directly locate targets. However, they typically adopt an “always-crop” policy, focusing on *where* to look while neglecting *whether* zooming is needed. For visually simple tasks, this blind cropping wastes computation and often introduces background noise that misleads the model. Furthermore, they struggle to separate and locate targets accurately in complex, multi-object scenarios.

Our SvfEye framework addresses these limitations by introducing a decision-aware reasoning mechanism. Rather than forcing the model to crop every time, we unify token-level confidence with semantic attention maps. The token confidence acts as a zero-cost switch to determine *whether* local visual details are needed before any action is taken. If required, the semantic attention maps then dictate exactly *where* to extract the features. By deciding before acting, our approach eliminates the latency of search-based methods and the computational redundancy of attention-based methods, achieving highly efficient and precise visual reasoning.

### 2.3. Confidence Estimation and Adaptive Inference

Confidence estimation allows models to evaluate their own uncertainty. In Large Language Models (LLMs), token-level probabilities serve as simple and effective indicators of how confident the model is about its predictions [5, 32]. When a model shows low confidence, it is more likely to hallucinate or make reasoning errors. Recent studies have introduced various methods to quantify this uncertainty, such as aggregating token probabilities [29] or calculating entropy [28], essentially helping models “know what they don’t know.”

While confidence signals are widely used in text generation, they are rarely applied to optimize how Multimodal Large Language Models (MLLMs) process images. Currently, many training-free MLLMs blindly extract high-resolution local details for every input, wasting massive computation on visually simple tasks. To address this, we employ token confidence as a zero-cost decision switch. By evaluating the confidence score from the initial global image, our framework autonomously decides *when* to fuse local visual context. If the model is confident, it answers directly; if uncertain, it selectively extracts and integrates fine-grained local details. This adaptive strategy completely avoids indiscriminate fusion, reduces background noise, and significantly accelerates inference.

## 3. Methods

### 3.1. Analysis: When and Where to Fuse

Before introducing SvfEye, we systematically analyze the fundamental limitations of existing training-free methods in determining *when* and *where* to extract local visual context for fusion. Our analysis aims to answer two critical questions: (1) Can models know when additional visual fusion is necessary? (2) What causes attention-based localization to fail on fine-grained tasks?

### 3.1.1. Can MLLMs know when to fuse local details?

In the **Thinking with Images** paradigm, some work enables models to decide **when to fuse** via reinforcement learning, whereas most training-free methods adopt indiscriminate extraction and fusion of local details for all samples, neglecting the critical question of **whether to fuse local visual sources**. For visually simple samples, such forced fusion incurs unnecessary computational overhead and inference latency, and can introduce redundant or noisy local information that misleads the model into incorrect answers. Figure 3 illustrates two typical issues caused by indiscriminate cropping. First, it introduces perceptual noise that misleads reasoning (left): fusing a highly salient “SLOW DOWN” sign tricks the model into identifying it as a prohibited action, overriding the correct global prediction. Second, it creates redundant computation (right): if the target (“cocoa”) is already clear in the global view, adding a cropped region provides no new information and only slows down inference.

Additional visual evidence is often expected to improve the prediction confidence of MLLMs. However, this assumption has not been systematically validated across different samples. To investigate this, we conduct a token-level confidence analysis before and after fusing cropped regions. Based on the confidence change after multi-scale visual context fusion, we categorize samples into two exclusive groups: (i) *Need Processing*, where confidence increases ( $Score_{crop} > Score_{org}$ ), and (ii) *No Need Processing*, where confidence remains unchanged or decreases ( $Score_{crop} \leq Score_{org}$ ). The confidence distributions of the two groups are shown in Figure 2.

As shown in Figure 2, the *Need Processing* and *No Need Processing* samples exhibit a clear separation in their original average confidence distributions. On both AOKVQA and POPE, the *No Need Processing* samples show higher initial confidence, indicating that the original image provides sufficient visual evidence for prediction. In contrast, the *Need Processing* samples are concentrated in lower-confidence regions, suggesting that fusing additional local visual information is more beneficial when the model’s initial prediction is uncertain.

This analysis reveals that fusing local details has a heterogeneous effect on model confidence: while some samples benefit from additional visual details, many show unchanged or even reduced confidence, which helps explain cases where originally correct predictions deteriorate after fusing extra local views. Importantly, the original confidence effectively reflects the model’s need for additional visual evidence, enabling a simple and reliable criterion for deciding **when to fuse local visual details**.

### 3.1.2. Limitations of Attention Maps in Fusion

Multimodal large language models (MLLMs) possess inherent visual grounding capabilities [31], and their spatial attention allows for more efficient visual localization compared to search-based methods (e.g., DC<sup>2</sup> [24] and ZoomEye [21]). However, relying solely on raw attention maps

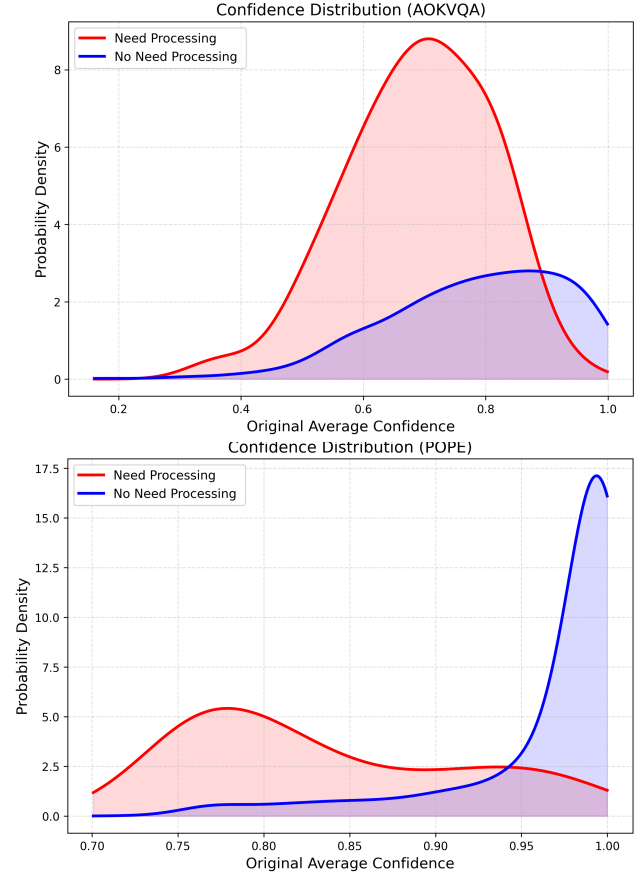


**Figure 2:** Probability density distributions of original average confidence on the AOKVQA and POPE datasets. The red curves denote the “Need Processing” group, where local cropping improves prediction confidence ( $Score_{crop} > Score_{org}$ ). The blue curves denote the “No Need Processing” group, where cropping brings no confidence gain ( $Score_{crop} \leq Score_{org}$ ).

presents two main challenges for precise fusion of semantic and visual information.

The first problem occurs when a question involves multiple objects (e.g., “Is the bicycle on the left or right side of the motorcycle?”). The model may fail to focus on the correct object because the attention is spread across several entities, causing imprecise localization. We address this by first extracting the main target from the question using few-shot in-context learning (ICL). The text tokens of this target are then used as queries in an attention mechanism over all image tokens, producing a target-guided attention map. This token-level fusion explicitly aligns textual and visual information, helping the model focus on the object of interest with greater precision.

The second problem happens when there are many objects of the same type close together (e.g., “How many people?”). The attention map often merges nearby objects into one region, making it hard to tell them apart. To solve this, we first apply a threshold to identify candidate regions, then remove overlapping or redundant regions with a simple

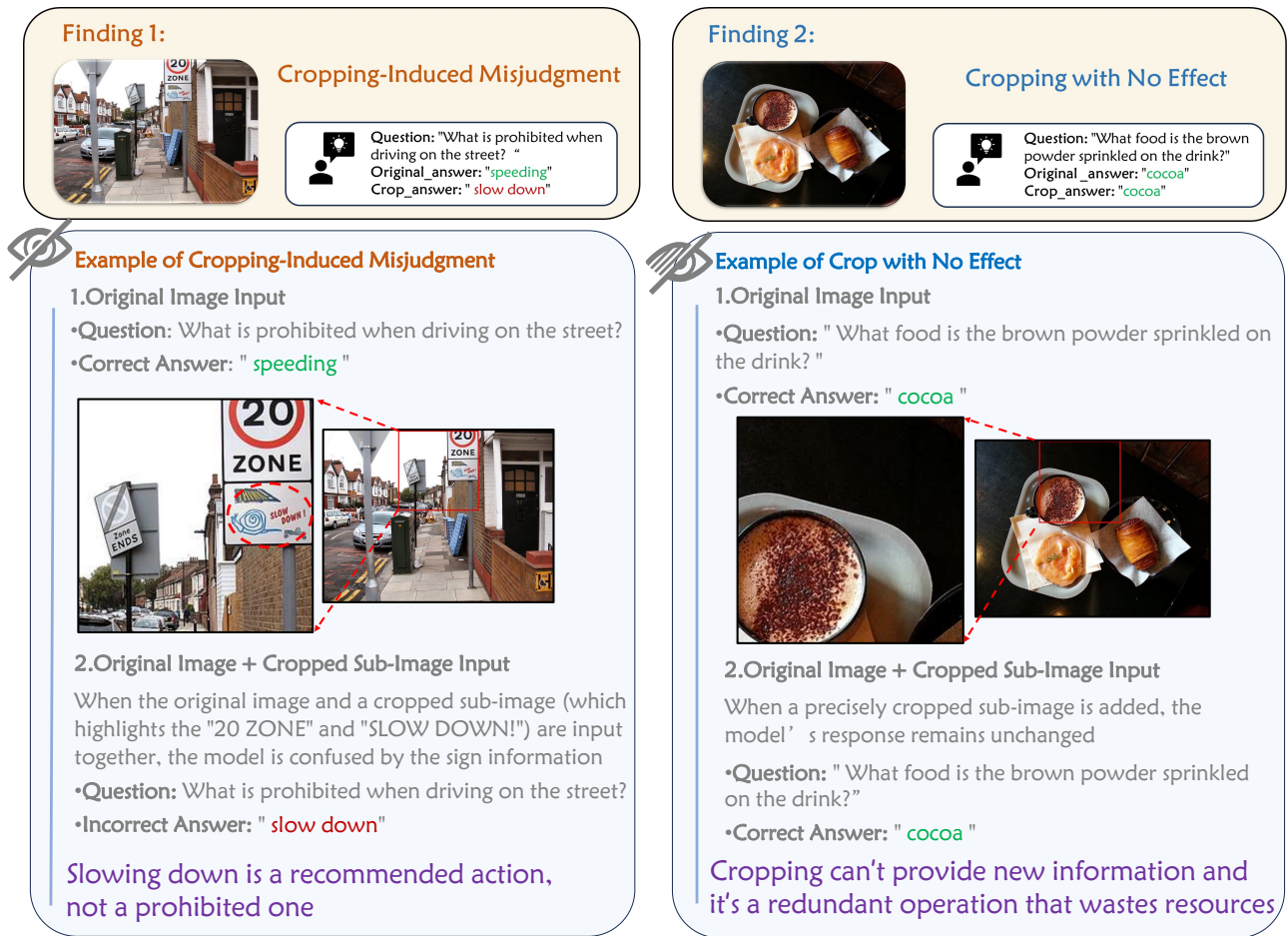


**Figure 3:** Limitations of indiscriminate image fusion. Left: Cropping a region containing the "SLOW DOWN" sign misleads the model to answer "slow down," even though the question asks what action is prohibited and the correct answer is "speeding." Right: Cropping the drink area adds no new visual information, but the model's prediction remains unchanged while additional computation is introduced.

spatial filtering step. The refined regions are then used to produce the final answer.

By addressing these two issues, the resulting attention map provides a more reliable way to locate the relevant visual regions, combining semantic cues from the question with visual attention to determine *where to fuse* in complex scenes.

### 3.2. SvfEye: Overview

To address the limitations of existing training-free methods, we propose **SvfEye**, a two-stage framework for efficient and adaptive visual-semantic fusion. The first stage is a *confidence-based module* that decides *when to fuse* additional local visual information, avoiding unnecessary processing for simple instances. The second stage is a *Semantic–Attention Fusion module* that determines *where to fuse* by integrating the semantic intent extracted from the question with the model's spatial attention, ensuring accurate localization of multiple objects. Together, these two stages form a pipeline that adaptively fuses local visual regions with global

context to enhance reasoning efficiency and accuracy. The overall workflow of SvfEye is illustrated in Figure 4.

### 3.3. Confidence-based Decision Module: "Determining When to Fuse"

For a given input image  $I$  and query  $Q$ , the model first performs an initial inference to obtain a preliminary answer sequence, denoted as  $Answer_{pre}$ . However, relying solely on the global view may be insufficient for all fine-grained reasoning requirements. To strike an optimal balance between improving model performance and conserving computational resources, we design a confidence-based decision module to determine whether to trigger a subsequent multi-scale fusion module. Unlike explicit prompting methods that require an additional generation step to make a routing decision, our strategy directly extracts the internal token probabilities from this initial forward pass. This allows the model to assess its own uncertainty with virtually zero extra computational cost, effectively avoiding the latency of redundant inference rounds.

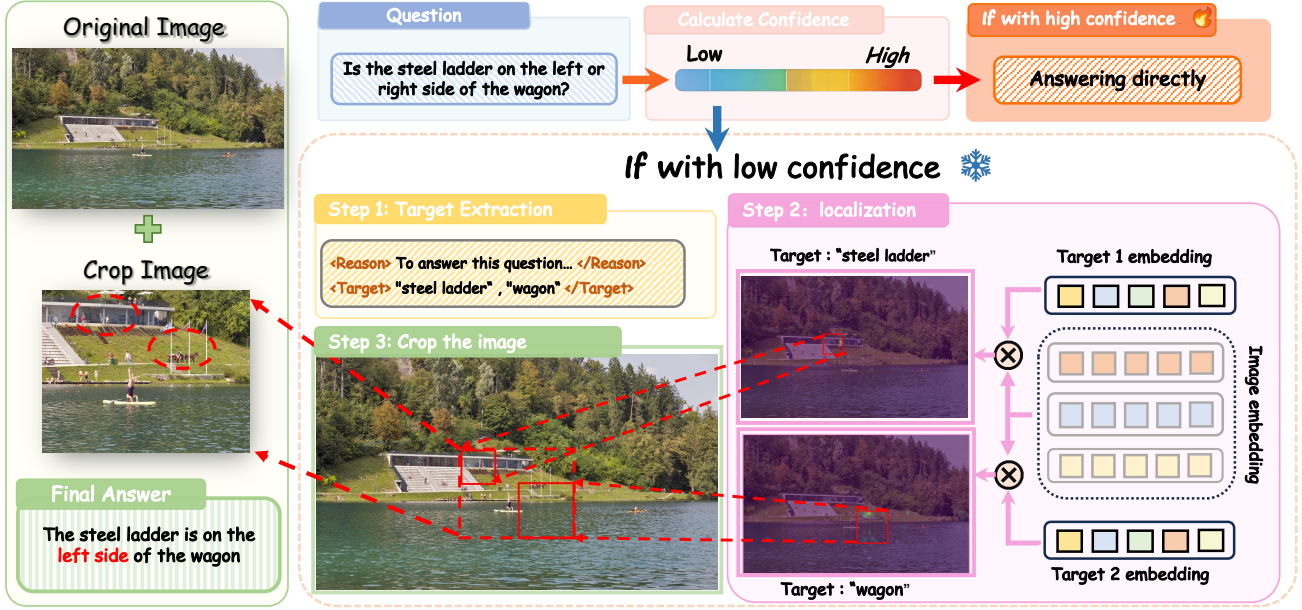


**Figure 4:** Overview of the SvfEye framework. The model evaluates token confidence to decide if local visual details are needed. If uncertain, it extracts key textual targets and uses them as queries in cross-attention over visual tokens for precise localization. These cropped regions are then fused with the global image to produce the final answer.

### 3.3.1. Model Confidence Quantification.

We quantify the confidence of the model by utilizing the average confidence of the tokens in the generated answer sequence. Specifically, the sequence is defined as

$$Y = \{y_1, y_2, \dots, y_T\}, \quad (1)$$

where  $y_t$  represents the  $t$ -th token, and  $P(y_t|\cdot)$  denotes the probability of the model generating this token at step  $t$ . We define the confidence score  $C$  as the arithmetic mean of the Softmax probabilities of all tokens in the sequence. This confidence score  $C$  intuitively reflects the model's epistemic uncertainty regarding the preliminary answer  $Answer_{pre}$ .

$$C = \frac{1}{T} \sum_{t=1}^T P(y_t|\cdot). \quad (2)$$

### 3.3.2. Optimal Threshold Selection.

A simple yet effective approach is to use a fixed decision threshold  $\tau$ . As demonstrated in Section 4.6, fusing local visual context only for samples with confidence scores below this threshold improves performance while reducing computational overhead.

When representative validation data are available and closely aligned with the test distribution, we further consider a principled threshold optimization strategy. Specifically, threshold selection is formulated as a statistical decision problem, where the optimal  $\tau$  is obtained by maximizing the following utility function:

$$J_\lambda(\tau) = \text{TPR}(\tau) - \lambda \cdot \text{FPR}(\tau), \quad \lambda > 0. \quad (3)$$

Here, TPR and FPR denote the true positive rate and false positive rate, respectively, and  $\lambda$  serves as a cost-weighting

hyperparameter that balances potential performance gains against the unnecessary fusion of local details.

This optimization strategy assumes access to representative validation data. **In open-domain settings where such data cannot be reliably obtained, employing a high fixed threshold remains a stable and effective alternative**, as evidenced by the results in Table 6. These observations further demonstrate the robustness and generalization capability of our approach.

### 3.3.3. Final Decision Process.

Based on the optimal decision boundary, we perform the following binary decision: (1)  $C \geq \tau$ : the model exhibits high confidence on the global view. In this case, we consider the available visual information sufficient for reasoning and directly output  $Answer_{pre}$  as the final answer. (2)  $C < \tau$ : the model shows high uncertainty, indicating that the current visual information may be insufficient to support fine-grained reasoning. We therefore trigger the subsequent fusion module to integrate local details.

## 3.4. Semantic-attention Fusion module: "Determining Where to Localize"

Upon triggering multi-scale visual context fusion, the model must precisely localize the target regions to extract details. However, relying exclusively on raw visual attention often leads to attention misalignment. In complex scenes or multi-object queries, unguided attention mechanisms frequently activate irrelevant backgrounds or conflate distinct instances.

To address this limitation, we introduce a semantic-attention fusion module that utilizes explicit language intent

to guide spatial localization. This process operates in two integrated steps: first, we decouple the pure semantic target from the complex user query to isolate the core physical subject; Second, the text tokens of the extracted target act as queries over all image tokens (keys and values), enabling a cross-attention that fuses the target semantics with the visual tokens and yields a target-guided attention map. This deep text-to-vision fusion successfully translates abstract language intent into a concrete bounding box for local detail extraction.

### 3.4.1. Semantic Decoupling (What to Localize).

To accurately extract key visual entities, We design a prompt template based on Chain-of-Thought. We guide the model to first generate a <Reason> tag before outputting the final <target>.

Formally, given a question  $Q$ , the model outputs a semantic target set  $E = \{e_1, e_2, \dots\}$ . For example, for "What kind of animal is on the red sign?", the model generates: <Reason>The question asks about something on a sign. The core subject to locate is the sign.</Reason><Target>red sign</Target>. Then it extracts  $E = \{\text{"red sign"}\}$ .

To illustrate this extraction capability across complex scenarios, we integrate a standardized prompt template and provide comprehensive few-shot examples, as shown below.

#### Target Extraction Prompt

##### Question Template:

Based on the question, identify ONLY the primary, physical objects or subjects mentioned. Do not include adjectives, locations, or states.

Please respond using <Reason> and <target> tags.

##### Guidelines:

- A 'target' must be a simple, concrete noun (e.g., 'car', 'person', 'table').
- For multiple distinct subjects, separate them with a comma (e.g., 'cat, dog').

**Question:** What is the brand name on the laptop?

**Response:** <Reason>The question asks about a brand name found on a laptop. The core physical subject is the laptop.</Reason><target>laptop</target>

**Question:** How many people are wearing hats in the image?

**Response:** <Reason>The question asks to count people who are wearing hats. The primary subjects are people and hats.</Reason><target>people, hats</target>

**Question:** Is the cat on the left or right side of the wooden chair?

**Response:** <Reason>The question asks about the position of a cat relative to a wooden chair. The core physical subjects are the cat and the chair.</Reason><target>cat, wooden chair</target>

**Question:** What kind of food is on the white plate?

**Response:** <Reason>The question asks about the type of food on a plate. The primary physical subjects are the food and the plate.</Reason><target>food, white plate</target>

**Question:** What is the man in the blue shirt holding in his hand?

**Response:** <Reason>The question asks about an object held by a man. The core physical subjects are the man and the object he is holding.</Reason><target>man, object</target>

**Question:** What time is displayed on the clock on the wall?

**Response:** <Reason>The question asks for the time displayed on a clock. The core physical subject is the clock.</Reason><target>clock</target>

### 3.4.2. Spatial Attention Mapping (Where to Localize).

After identifying the semantic target  $E$ , we use the extracted <target> to construct a localization prompt. By explicitly fusing this decoupled semantic intent with the visual spatial features, we ensure precise targeting and prevent the attention drift commonly caused by multi-object interference.

**2D Attention Map Generation.** Let  $Z_{\text{img}}$  denote the visual token sequence obtained from the image patches, and let  $Z_{\text{text}}^E$  denote the text tokens corresponding to the extracted target. We extract the cross-attention responses from the MLLM and average them across all attention heads:

$$A_{1D} = \text{Agg}(\text{Attn}(Z_{\text{text}}^E \rightarrow Z_{\text{img}})) \quad (4)$$

The resulting vector  $A_{1D}$  corresponds to the flattened visual token grid. We reshape it according to the patch layout of the vision encoder to obtain a 2D attention map  $A_{\text{map}} \in \mathbb{R}^{h \times w}$ , where each value indicates the attention intensity of the corresponding image region.

**Adaptive Multi-Scale Sliding Window.** Given the spatial attention map  $A_{\text{map}}$ , our goal is to translate this activation grid into a precise bounding box. To accommodate the variance in input resolutions, we dynamically set an adaptive base dimension  $S_{\text{base}}$  (typically  $224 \times 224$ , scaling to  $448 \times 448$  for ultra-high-resolution images) based on the original image size.

Building upon this adaptive base, we apply a predefined set of scaling ratios  $R = \{1.0, 1.2, 1.4, 1.6, 1.8, 2.0, 4.0, 6.0\}$ . For each ratio  $r \in R$ , the candidate extraction size is calculated as  $S_r = S_{\text{base}} \times r$ . This physical dimension is then projected onto the  $A_{\text{map}}$  grid to determine a corresponding window covering  $w_r \times h_r$  attention blocks. We slide this window across the 2D grid to find the position  $(x^*, y^*)$  that yields the maximum attention sum  $V_{\text{max}}$ .

To select the most fitting scale, we evaluate the *localization sharpness* (or contrast)  $\Delta_r$  for the peak window of each ratio. The sharpness is calculated by taking the difference between the peak attention  $V_{\text{max}}$  and the average attention of its four adjacent surrounding windows  $V_{\text{adj}}$ , normalized by the window area:

$$\Delta_r = \frac{V_{\text{max}} - \text{Mean}(V_{\text{adj}})}{w_r \times h_r} \quad (5)$$

Intuitively, a higher  $\Delta_r$  means the window tightly encapsulates the highly activated target while excluding the unactivated background. We select the optimal ratio  $r^*$  that maximizes this sharpness metric.

**Coordinate Mapping.** Once the optimal grid window is found, we calculate its geometric center and linearly map it back to the original high-resolution image space. Based on the selected box size, we deduce the final pixel coordinates  $(x_1, y_1, x_2, y_2)$  and clamp them to the image boundaries. The original image  $I$  is then cropped accordingly to produce a detail-preserving local view  $I_{\text{crop}}$  for the subsequent local-global fusion.

### 3.4.3. Dealing with Multi-instances.

For queries involving multiple instances of the same category (e.g., "How many people?"), we introduce an attention-based post-processing scheme to separate closely spaced targets. Specifically, an attention score threshold is applied to filter foreground regions, with high-response areas identified as candidate boxes. To remove highly overlapping boxes, we apply an NMS-inspired [18] deduplication step: boxes with an IoU greater than 0.5 are treated as duplicates and pruned. This process effectively reduces spatial redundancy, enabling accurate localization and counting of individual objects.

## 4. Experiment

### 4.1. Implementation Details

**Experimental Setup & Network Configuration.** To validate the effectiveness of our approach, we integrate the SvfEye framework with two widely-used open-source models: Qwen2.5VL-3B [1] and LLaVA-1.5-7B [17]. In our experiments, we set the maximum input resolution for Qwen to 3,211,264 pixels. All experiments are conducted on NVIDIA H200 GPUs. For attention map acquisition, we extract attention scores from specific layers to isolate visual regions relevant to the target entity. Specifically, for Qwen2.5-VL, we extract attention scores from Layer 22, utilizing the last token of the target sequence as the query. For LLaVA-1.5, we use attention weights from Layer 14, averaging the attention scores of all tokens comprising the final word of the target phrase to create a stable spatial representation. We conduct a comprehensive comparison against both the original baselines and several state-of-the-art methods, including training-free approaches (e.g., ZoomEye [21], MLLMs-Know [31], DC<sup>2</sup> [24], and ViCrop [30]) and training-based models (e.g., PixelReasoner [22]).

**Datasets and Benchmarks.** We evaluate our model across various dimensions using four benchmarks. First, we select AOKVQA [20] and POPE [13] to assess general reasoning capabilities on knowledge-intensive tasks. Furthermore, to validate the effectiveness of our confidence-based decision module on fine-grained features, we introduce two challenging high-resolution datasets: **V\*-Bench** [27] and **HR-Bench** [24]. These benchmarks emphasize fine-grained attribute recognition and complex spatial reasoning, strictly evaluating the model's ability to localize tiny visual details.

### 4.2. Qualitative Analysis of Semantic-Attention Fusion

To visually demonstrate the effectiveness of our **Where to Localize** mechanism, we compare the attention maps and final bounding regions generated by SvfEye with those from a baseline attention-based localization method (MLLMs-Know).



**Figure 5:** Comparison of localization precision. The baseline model often suffers from single-target bias (A) and attention drift (C). In contrast, our method explicitly decouples multiple semantic targets to ensure complete coverage (B) and accurately identifies the intended subject (D). The attention maps demonstrate that our approach prevents noisy activations and maintains precise spatial focus.

#### 4.2.1. Accurate multi-object localization:

In Figure 5(A), the baseline suffers from a single-object bias, attending only to the 'steel ladder' while missing the 'wagon'. In contrast, SvfEye explicitly decouples multiple targets, activating both the 'steel ladder' and 'wagon'. As shown in Figure 5(B), the resulting union of bounding boxes effectively covers both objects, providing the MLLM with a complete and precise local visual source to accurately reason about their spatial relationship.

#### 4.2.2. Robust target identification:

In Figure 5(C), the baseline's attention drifts to the dominant adult in the scene (incorrect target). Guided by our prompt-driven target extraction, SvfEye accurately focuses on the "child", ensuring the extracted region aligns with the intended semantic target, as shown in Figure 5(D). These qualitative results demonstrate that fusing explicit target semantics with visual attention significantly mitigates attention diffusion and drift, ensuring that the "thinking with images" process relies on highly accurate visual evidence.

Model	Method	Training-free	AOKVQA	POPE	V* Bench	HR-Bench 4K	HR-Bench 8K
LLaVA-v1.5-7B	Baseline* [17]	✓	71.00	86.98	48.68	36.13	32.13
	DC <sup>2</sup> [24]	✓	-	-	57.60	-	39.50
	VisCrop [30]	✓	-	-	62.30	46.25	35.75
	MLLMs-Know* [31]	✓	72.31	87.25	56.02	44.38	37.25
	ZoomEye [21]	✓	70.56	88.94	83.25	49.88	48.63
	<b>Ours (SvfEye)</b>	✓	72.90	87.37	62.80	47.38	42.00
<b>Δ vs. Baseline</b>			<b>+1.90</b>	<b>+0.39</b>	<b>+14.12</b>	<b>+11.25</b>	<b>+9.87</b>
Qwen2.5VL-3B	Baseline* [1]	✓	71.44	87.20	75.90	67.50	58.88
	Pixel Reasoner [22]	✗	-	-	84.82	-	66.00
	MLLMs-Know* [31]	✓	71.62	89.12	75.90	66.36	64.88
	ZoomEye [21]	✓	71.26	88.93	89.01	70.13	68.38
	<b>Ours (SvfEye)</b>	✓	73.10	89.12	86.38	73.25	70.00
	<b>Δ vs. Baseline</b>			<b>+1.66</b>	<b>+1.92</b>	<b>+10.48</b>	<b>+5.75</b>

**Table 1**

**Comparison with state-of-the-art methods.** Highest results are marked in darker colors (Blue for LLaVA, Red for Qwen). The gray rows show the absolute improvement ( $\Delta$ ) of Ours over the Baseline. \* Results are reproduced by us using official implementations.

### 4.3. Quantitative Analysis

Our method shows strong performance on benchmarks that heavily test fine-grained visual details, such as HR-Bench and V\*-Bench. Although LLaVA operates at a fixed resolution, which naturally restricts its attention granularity, our approach still drives notable improvements: **+11.25%** on HR-Bench 4K, **+9.87%** on 8K, and **+14.12%** on V\*-Bench. Furthermore, when integrated with the Qwen2.5-VL backbone, our model reaches a state-of-the-art **70.00%** on HR-Bench 8K. This exceeds the baseline by **11.12%** and comfortably surpasses ZoomEye (65.63%). These quantitative gains demonstrate that our semantic-visual fusion effectively breaks through standard resolution bottlenecks. Moreover, this approach allows the model to adaptively focus on regions that contribute most to the task, avoiding unnecessary computation on irrelevant areas.

For reasoning-heavy benchmarks (AOKVQA, POPE), improvements are moderate, indicating that the primary challenge here lies in logical deduction rather than visual recognition. However, the consistent boost, pushing Qwen2.5-VL to **73.10%** on AOKVQA, highlights the advantage of our confidence-based mechanism over indiscriminate fusion of local details. By fusing local details *only when beneficial*, this strategy acts as a **semantic safeguard**: it clarifies local details without severing the global context, thus breaking the resolution bottleneck. Overall, these findings show the flexibility of our approach: it effectively **overcomes resolution limits** in perception tasks while keeping the core meaning needed for complex reasoning, demonstrating robustness across both visually demanding and reasoning-intensive scenarios.

### 4.4. Efficiency analysis

#### 4.4.1. Overall Inference Efficiency

Inference efficiency is an important factor for training-free methods. We evaluate SvfEye against two representative

baselines: **ZoomEye** (the current SOTA) and **MLLMs-Know** (an attention-based method). ZoomEye organizes the image into a hierarchical tree and performs iterative search to simulate zooming. Although effective, this global traversal becomes increasingly expensive. As shown in Figure 6, processing HR-Bench 8K requires more than 10 hours.

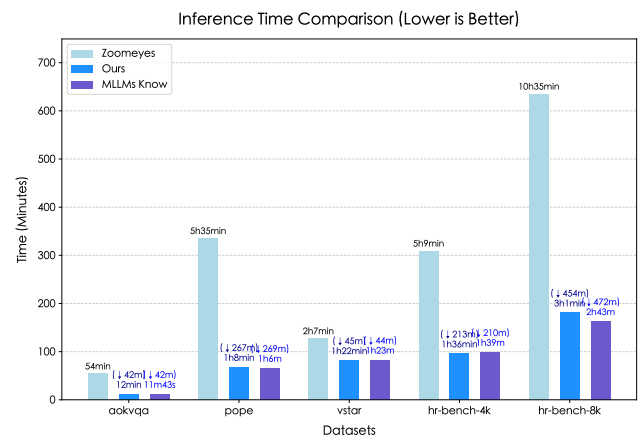


**Figure 6:** Comparison of total GPU inference time (in minutes) across different methods (measured on NVIDIA H200 GPUs).

In contrast, SvfEye localizes informative regions directly by fusing explicit target semantics with visual attention, avoiding exhaustive search over the full image. On HR-Bench 8K, this yields an approximately 4.0 $\times$  speedup compared with ZoomEye, while maintaining competitive performance.

Furthermore, SvfEye runs at a similar speed to MLLMs-Know across all evaluated datasets, while achieving higher accuracy on challenging high-resolution benchmarks. For example, SvfEye reaches 86.38% on V\*-Bench and 70.00%

on HR-Bench 8K, compared to 75.90% and 64.88% achieved by MLLMs-Know, respectively. These results suggest that the improvement mainly comes from a more effective allocation of computation for adaptive semantic-visual fusion, rather than increased inference cost.

#### 4.4.2. Contrast with LLM-Prompting Strategy

An intuitive alternative to our decision strategy is to directly prompt the MLLM to make the choice (e.g., asking "Do you need to extract and fuse fine-grained local details to answer this question? Answer Yes or No"). However, we demonstrate that utilizing token confidence is significantly more efficient than direct prompting.

To clearly illustrate the efficiency gap, we compare the inference pipelines of both methods in Algorithm 1.

#### Algorithm 1 Inference Workflow: LLM-Prompting vs. Ours

```

1: # Method 1: LLM-Prompting
2: Decision ← LLM_Generate( $I_{global}$ , "Need local details?")
3: if Decision == "No" then
4:   # Still requires 1 round to answer
5:   Return LLM_Generate( $I_{global}$ , Question)
6: else
7:   # Decision is "Yes": Extract local details via attention
8:    $I_{local}$  ← Semantic_Guided_Extract( $I_{global}$ )
9:   Return LLM_Generate( $I_{global}$ ,  $I_{local}$ , Question)
10: end if

11: # Method 2: Ours (Token Confidence)
    LLM_Generate( $I_{global}$ , Question)
12: if Confidence(Logits) ≥ Threshold then
13:   # High confidence: Answer directly
14:   Return Answer
15: else
16:   # Low confidence: Extract local details via attention
17:    $I_{local}$  ← Semantic_Guided_Extract( $I_{global}$ )
18:   Return LLM_Generate( $I_{global}$ ,  $I_{local}$ , Question)
19: end if

```

As shown in Algorithm 1, the LLM-Prompting approach requires a strictly sequential pipeline. The model must explicitly generate a text-based decision before solving the actual task. Consequently, even for simple queries that do not require multi-scale visual context fusion, the model wastes valuable computational resources and time performing an additional LLM\_Generate step just to output "No".

In contrast, our Token Confidence method avoids this bottleneck by attempting to answer the question directly. We calculate the confidence score from the internal probability distribution (Softmax logits) of this first attempt. Since these logits are generated automatically during the forward pass, obtaining the confidence score costs virtually zero extra time. If the confidence is high, we directly output the initial answer, bypassing the need for a second inference round entirely.

**Table 2**

Total inference time comparison between LLM-Prompting and our Token Confidence decision mechanisms (measured on NVIDIA H200 GPUs).

Decision Mechanism	AOKVQA	POPE	V*-Bench	HR 4K	HR 8K
LLM-Prompting	16m45s	1h33m	1h29m	1h47m	3h06m
Ours (Confidence)	12m33s	1h08m	1h22m	1h36m	3h01m

To empirically validate this workflow advantage, we compare the total inference time of the two decision mechanisms. As shown in Table 2, our strategy is consistently faster across all benchmarks under identical hardware conditions. The efficiency gains are particularly pronounced on general reasoning datasets (e.g., saving 25 minutes on POPE, a 26.8% reduction), where a large portion of queries can be answered using only the global view. Even on challenging datasets like HR-Bench 8K where multi-scale visual context fusion is frequently triggered, our method still reduces overall latency by completely eliminating the redundant "Yes/No" token generation step.

## 4.5. Ablation study

### 4.5.1. Ablation on Confidence-based Decision module

As shown in Table 3, our confidence-based decision module consistently improves accuracy compared to indiscriminate cropping (*w/o confidence-based decision*). For Qwen2.5-VL, our strategy yields a +1.14% on AOKVQA and +0.52% on V\*-Bench. This confirms that indiscriminate cropping introduces visual noise and misjudgments, which our selective strategy effectively avoids.

**Table 3**

Quantitative evaluation of confidence-based decision module.

Model	AOKVQA	V*-Bench
Qwen2.5VL-3B		
<i>w/o confidence-based decision</i>	71.96%	85.86%
<i>w/ confidence-based decision</i>	<b>73.10%</b>	<b>86.38%</b>
$\Delta$	<b>+1.14%</b>	<b>+0.52%</b>

Table 4 demonstrates the efficiency of our confidence-based decision module. On AOKVQA, we are able to skip redundant cropping for 67.60% of the samples, effectively halving the inference time without compromising accuracy. Interestingly, this adaptive approach achieves even higher accuracy than applying full cropping (+1.14), indicating that it successfully avoids the interference noise that can arise from unnecessary fusion of local details. For more challenging benchmarks such as V\*-Bench, the model naturally performs cropping more frequently, yet it still manages to reduce redundant processing by 22.52% while sustaining strong performance. These results highlight that SvfEye dynamically adjusts its processing behavior according to task complexity, providing a robust and practical trade-off between computational efficiency and predictive accuracy.

**Table 4**

Performance and efficiency comparison (measured on NVIDIA H200 GPUs).

Benchmark	Acc	Time	Crop%
AOKVQA			
w/o confidence-based decision	71.96	26m24s	100%
w/ confidence-based decision	<b>73.10</b>	<b>12m33s</b>	32.40%
$\Delta$	<b>+1.14</b>	<b>-13m51s</b>	<b>-67.60%</b>
V*-Bench			
w/o confidence-based decision	85.86	1h04m	100%
w/ confidence-based decision	<b>86.38</b>	1h18m	77.48%
$\Delta$	<b>+0.52</b>	<b>+14m</b>	<b>-22.52%</b>

#### 4.5.2. Ablation on Semantic-attention Fusion

**Table 5**

Ablation on Semantic-attention Fusion Module.

Model & Strategy	AOKVQA	POPE	V*-Bench	HR 4K	HR 8K
LLaVA-v1.5-7B					
w/o Semantic-attention Fusion	72.31%	87.25%	56.02%	44.38%	37.25%
w/ Semantic-attention Fusion	<b>72.90%</b>	<b>87.37%</b>	<b>62.80%</b>	<b>47.38%</b>	<b>42.00%</b>
$\Delta$	0.59%	0.12%	<b>6.78%</b>	<b>3.00%</b>	<b>4.75%</b>
Qwen2.5VL-3B					
w/o Semantic-attention Fusion	71.62%	<b>89.12%</b>	75.90%	66.36%	64.88%
w/ Semantic-attention Fusion	<b>71.96%</b>	<b>89.12%</b>	<b>85.86%</b>	<b>72.50%</b>	<b>70.00%</b>
$\Delta$	0.34%	–	<b>9.96%</b>	<b>6.14%</b>	<b>5.12%</b>

To validate the effectiveness of the Semantic-attention Fusion module, we compare model performance with and without this component (Table 5). The quantitative results reveal a clear distinction depending on the task requirements.

On standard visual reasoning datasets (AOKVQA and POPE), the performance improvements are marginal. This is reasonable, as these benchmarks primarily emphasize complex logical reasoning and commonsense knowledge rather than the perception of fine-grained visual details. For such tasks, the bottleneck typically lies in the reasoning capabilities of the language model rather than visual clarity. Since the base global encoding already captures the necessary semantic elements to support this reasoning, extracting high-resolution local crops provides limited additional benefit.

However, on high-resolution and detail-oriented benchmarks (V\*-Bench, HR 4K, and HR 8K), the module provides substantial gains. When processing complex scenes, base models often fail to capture small target objects. By incorporating our module, LLaVA-v1.5 improves by 6.78% on V\*-Bench and 4.75% on HR 8K. The impact is even more pronounced for Qwen2.5-VL, which achieves a 9.96% boost on V\*-Bench and a 6.14% increase on HR 4K.

These consistent improvements across different model architectures demonstrate the core advantage of the proposed module. By explicitly using semantic intent to guide visual attention, the module effectively isolates and extracts the exact query-relevant regions. This mechanism prevents background noise from interfering with the reasoning process, proving crucial for accurately localizing fine-grained details in complex, high-resolution scenes.

## 4.6. Confidence Sensitivity Analysis

To evaluate the robustness of our confidence-based decision module, we conduct a sensitivity analysis aligned with the two scenarios introduced in subsection 3.3: optimizing the decision threshold via the utility function, and applying direct fixed thresholds for open-domain settings.

### 4.6.1. Threshold Optimization via Utility Function

**Table 6**

Sensitivity Analysis of the confidence-based decision module.

Model	Baseline	Full Fusion (All Fuse)	Confidence-based Decision ( $\lambda$ )			Fixed Thresh. ( $\tau = 0.92$ )
	(Original)		1.0	1.5	2.0	
Threshold ( $\tau$ )	-	-	0.830	0.734	0.533	0.92
Qwen2.5-VL	71.44	71.96	72.58	<b>73.10</b>	72.49	72.05

In our formulation, the decision of whether to extract and fuse local sources relies on the utility function  $J_\lambda(\tau) = \text{TPR}(\tau) - \lambda \cdot \text{FPR}(\tau)$ . The hyperparameter  $\lambda$  serves as a cost-weighting factor that balances the expected benefit of correctly fusing local details against the potential risk of unnecessary computational redundancy. Specifically, larger values of  $\lambda$  impose stronger penalties on false-positive decisions, encouraging a more conservative fusion policy (i.e., yielding a lower optimal threshold  $\tau$ ). Conversely, smaller values of  $\lambda$  favor more aggressive multi-scale visual context fusion to ensure the capture of fine-grained visual details, thereby expanding the triggering region by adopting a higher threshold.

When representative validation data is available,  $\lambda$  can be tuned to maximize task-specific performance. We analyze this optimization on the AOKVQA benchmark by varying  $\lambda$ . As shown in Table 6, the performance peaks at 73.10% when  $\lambda = 1.5$ , which derives an optimal threshold of  $\tau = 0.734$ . Notably, this dynamically optimized approach clearly outperforms both the original baseline (71.44%) and the rigid ‘‘Full Fusion’’ strategy (71.96%). This performance gap indicates that indiscriminate zooming not only wastes computational resources but can also introduce visual noise that degrades reasoning. Ultimately, this confirms that our algorithm successfully finds a favorable trade-off between extracting necessary fine-grained details and preventing redundant fusion.

### 4.6.2. Threshold Robustness in Open-Domain Settings

In real-world open-domain scenarios, it is often impractical to carefully tune the hyperparameter  $\lambda$  due to the lack of validation data. To evaluate whether our framework can still perform reliably without such tuning, we sweep across a range of threshold values  $\tau$  (see Table 7). The results show that our method is not sensitive to the exact choice of the threshold. Even without precise calibration, the model maintains stable performance, and its accuracy consistently remains above the baseline across a wide range of relatively high thresholds (e.g.,  $\tau \in [0.94, 1.00]$ ).

**Table 7**

Sensitivity analysis across multiple benchmarks under varying confidence thresholds  $\tau$ .

Dataset	Base	random		continuous			
		0.80	0.90	0.94	0.96	0.98	1.00
HR-4K	67.50	72.75	72.50	72.75	72.50	72.50	72.50
HR-8K	58.88	68.25	69.88	<b>70.00</b>	<b>70.00</b>	<b>70.00</b>	<b>70.00</b>
V*-Bench	75.90	81.15	84.81	<b>86.38</b>	<b>86.38</b>	85.86	85.86
AOKVQA	71.44	72.31	<b>72.40</b>	72.23	72.23	72.14	71.97

#### 4.6.3. Robustness with a fixed Threshold

**Table 8**

Evaluation under a fixed threshold ( $\tau = 0.96$ )

Benchmark	Baseline	$\tau = 0.96$	Extraction Reduced
AOKVQA	71.44	72.23	10.39%
V*-Bench	75.90	86.38	14.13%
HR-Bench 8K	58.88	70.00	8.00%
HR-Bench 4K	67.50	72.50	10.00%
<b>Average <math>\Delta</math></b>	–	<b>+9.35%</b>	<b>10.63%</b>

Building on the observed stability, we evaluate a single, conservative fixed threshold ( $\tau = 0.96$ ) across all datasets without any per-task adjustment (Table 8). Under this strictly unified zero-shot setting, SvfEye consistently outperforms the baseline, achieving an average accuracy gain of **+9.35%**. Simultaneously, it bypasses redundant fusion to reduce processed image regions by an average of **10.63%**. This confirms that SvfEye can function as a highly robust, plug-and-play module that adapts to diverse tasks using just a simple, high fixed threshold.

## 4.7. Discussion & Generalization

### 4.7.1. Detailed Performance Analysis on V\*-Bench

While SvfEye demonstrates strong performance across most benchmarks, we provide a deeper analysis of its behavior on V\*-Bench, focusing on the specific challenges posed by representation constraints and complex spatial reasoning tasks.

**Resolution and Representation Constraints.** LLaVA-v1.5 processes images at a fixed resolution of  $336 \times 336$ , which limits the level of visual detail the model can capture. For benchmarks such as V\*-Bench that contain many extremely small objects, this resolution becomes a clear limitation. Since each visual token corresponds to a relatively large image region, the resulting attention maps are inherently coarse. As a result, the model often lacks the precision needed to localize very small targets and produce tight bounding boxes. This limitation is reflected in the much stronger performance observed when using the Qwen2.5-VL. By supporting dynamic high-resolution inputs (up to 3.2M pixels), Qwen2.5-VL provides more detailed visual representations, leading to more precise attention maps and more accurate cropping decisions.

**Efficiency vs. Spatial Reasoning Trade-off.** V\*-Bench heavily features spatial reasoning and visual search queries,

such as determining the relative positions of distant objects. While SvfEye successfully localizes multiple individual targets, it generates relatively tight bounding boxes around them. When objects are extremely far apart, localizing tightly around them may inadvertently discard the surrounding contextual information necessary for inferring broad relational tasks.

In contrast, search-based methods like ZoomEye utilize a recursive tree-search: they iteratively split the image into sub-regions, verify targets, and merge confident regions into a single large composite image. This exhaustive approach makes them more robust for complex spatial queries but incurs massive computational overhead (as demonstrated in our efficiency analysis, ZoomEye suffers from an approximately **4.0 $\times$**  latency increase). Overall, SvfEye maintains competitive average performance while operating significantly faster. The performance gap on specific V\*-Bench spatial queries primarily reflects a deliberate algorithmic trade-off: SvfEye prioritizes inference efficiency and precise targeted semantic-visual fusion over exhaustive global search, rather than a fundamental limitation of our semantic-attention fusion module.

### 4.7.2. Case Studies on Semantic-Visual Fusion

We provide qualitative examples (Figure 7–Figure 8) to demonstrate how our semantic-visual fusion effectively resolves challenging queries.

**Fine-Grained and Small Object Perception.** Small visual details are inherently compressed and easily lost in standard global low-resolution views. For instance, identifying a minute “spider” logo on a sail or a low-contrast bag in a dimly lit street (Figure 7) is highly challenging for baseline models. SvfEye solves this by decoupling the core textual targets (“blue sail”, “bag”) and fusing them with visual spatial features to accurately localize these subtle objects. By extracting and fusing these high-resolution local crops back into the global context, Our framework integrates local visual context with global context, preserving the necessary fine-grained features for accurate prediction.

**Multi-Target Spatial Reasoning.** Questions requiring relative position comprehension often cause severe attention drift in standard models, leading them to focus on a single dominant object or irrelevant background noise. When asking whether a “baby stroller” is to the left or right of a “person in orange” (Figure 8), our method explicitly decouples the two entities to prevent this bias. Each textual target is individually fused with the spatial attention map to generate a corresponding bounding box. The resulting regions are then merged through a spatial union operation to obtain a unified, noise-free local view that covers both subjects. This localized region is subsequently integrated with the global context, preserving the precise spatial relationship while filtering out visual distractors, ultimately enabling more reliable spatial reasoning.

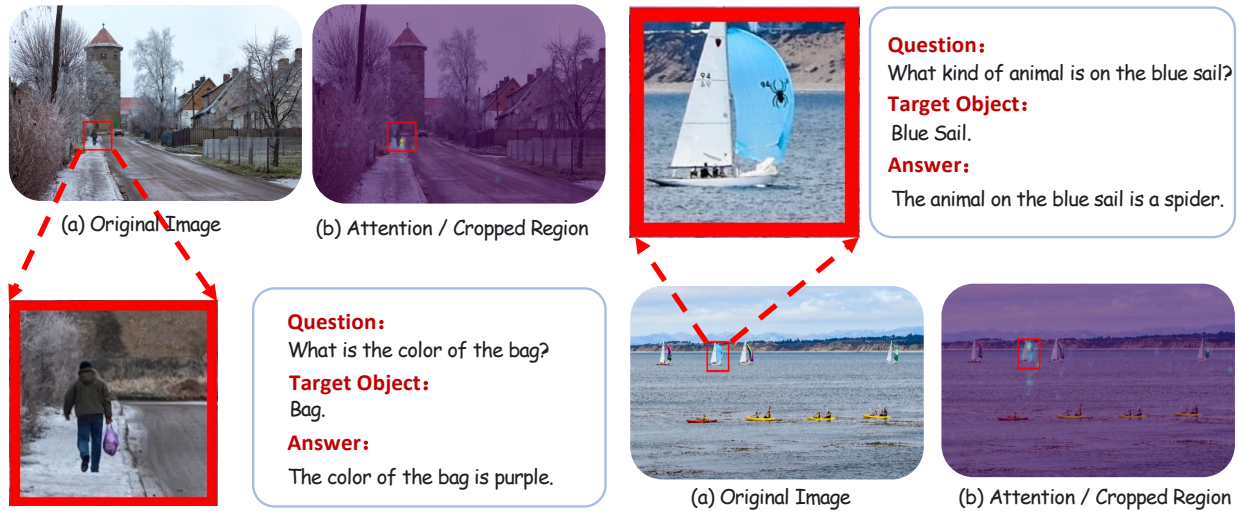


**Figure 7: Qualitative examples of semantic-visual fusion.** Left: For small object perception, SvfEye precisely targets the “Bag” to identify its purple color despite a complex background. Right: For fine-grained attribute recognition, the model isolates the “Blue Sail” to accurately reveal the subtle spider logo.

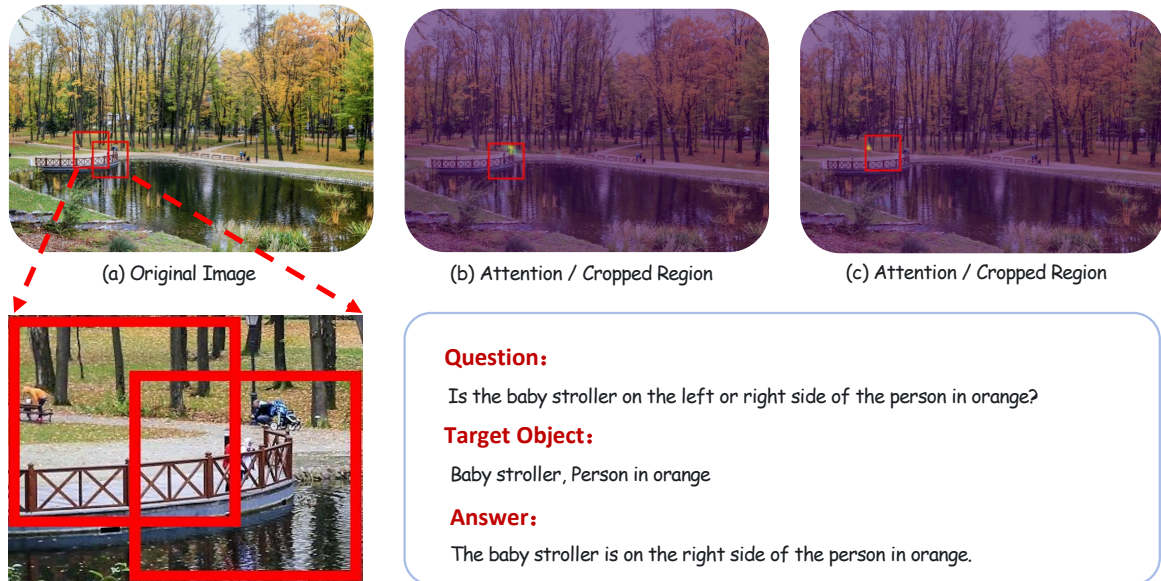


**Figure 8: Spatial Reasoning with Multiple Targets.** The model attends to both the “Baby stroller” and the “Person in orange,” extracting a region that preserves their relative spatial position.

## 5. Conclusion

We propose SvfEye, a training-free semantic-visual fusion framework that leverages multi-scale visual context to improve fine-grained reasoning in MLLMs. While integrating local sub-images helps models capture subtle visual details, existing methods typically fuse these regions unconditionally, introducing perceptual noise and computational waste. In contrast, SvfEye adaptively determines *when* and *where* to incorporate local information.

First, to mitigate the perceptual noise caused by blind fusion, we introduce a confidence-based fusion module. In

many cases, the global view alone is sufficient for answering simple queries. SvfEye therefore estimates the model’s uncertainty based on the token confidence obtained from the initial global reasoning stage and determines *when* local details are needed. When confidence is low, local regions are extracted and fused into the global context to support further reasoning. This strategy effectively reduces redundant computation while improving the accuracy. Second, to address the attention drift problem in current localization methods, we introduce a semantic-visual fusion module to determine *where* to localize. Pure visual attention is easily distracted by irrelevant backgrounds or similar objects. To prevent this, our method extracts explicit text targets from

the query to serve as the query token in a text-to-image attention mechanism. This semantic-visual fusion ensures that the model accurately locates and integrates only the relevant regions.

Extensive experiments demonstrate that SvfEye achieves SOTA performance across multiple challenging benchmarks while maintaining high inference efficiency. As a plug-and-play module that requires no parameter updates, it generally works well in various MLLM architectures. In general, the semantic-visual fusion framework effectively alleviates perceptual redundancy and spatial attention drift, highlighting the importance of cross-modal fusion in addressing the perception limitations of current MLLMs.

## CRedit authorship contribution statement

**Yuxiang Shen:** Writing–review & editing, Experiment. **Hailong Huang:** Writing–review, Methodology, Investigation, Software. **Zhenkun Gao:** Writing–review, Validation, Software. **Xueheng Li:** Writing–review, Formal analysis, Validation. **Man Zhou:** Supervision, Writing–review & editing, Conceptualization. **Chengjun Xie:** Supervision, Writing–review & editing. **haoxuan che:** Supervision, Investigation, Writing–review & editing. **Xuanhua He:** Supervision, Investigation, Writing–review & editing. **Jie Zhang:** Supervision, Writing–review & editing.

## References

- [1] Bai, S., Chen, K., Liu, X., Wang, J., Ge, W., Song, S., Dang, K., Wang, P., Wang, S., Tang, J., et al., 2025. Qwen2.5-vl technical report. arXiv preprint arXiv:2502.13923 .
- [2] Chen, Z., Wu, J., Wang, W., Su, W., Chen, G., Xing, S., Zhong, M., Zhang, Q., Zhu, X., Lu, L., et al., 2024. Internvl: Scaling up vision foundation models and aligning for generic visual-linguistic tasks, in: Proceedings of the IEEE/CVF conference on computer vision and pattern recognition, pp. 24185–24198.
- [3] Comanici, G., Bieber, E., Schaekermann, M., Pasupat, I., Sachdeva, N., Dhillion, I., Blistein, M., Ram, O., Zhang, D., Rosen, E., et al., 2025. Gemini 2.5: Pushing the frontier with advanced reasoning, multimodality, long context, and next generation agentic capabilities. arXiv:2507.06261 .
- [4] Dai, W., Li, J., Li, D., Tiong, A., Zhao, J., Wang, W., Li, B., Fung, P.N., Hoi, S., 2023. Instructblip: Towards general-purpose vision-language models with instruction tuning. Advances in neural information processing systems 36, 49250–49267.
- [5] Fadeeva, E., Rubashevskii, A., Shelmanov, A., Petrakov, S., Li, H., Mubarak, H., Tsymbalov, E., Kuzmin, G., Panchenko, A., Baldwin, T., et al., 2024. Fact-checking the output of large language models via token-level uncertainty quantification, in: Findings of the Association for Computational Linguistics: ACL 2024, pp. 9367–9385.
- [6] Gao, Z., Wang, X., Tan, X., Xie, Y., 2026. Tpru: Advancing temporal and procedural understanding in large multimodal models. arXiv preprint arXiv:2602.18884 .
- [7] Hosseini, A., Yuan, X., Malkin, N., Courville, A., Sordani, A., Agarwal, R., 2024. V-star: Training verifiers for self-taught reasoners. URL: <https://arxiv.org/abs/2402.06457>, arXiv:2402.06457.
- [8] Hurst, A., Lerer, A., Goucher, A.P., Perelman, A., Ramesh, A., Clark, A., Ostrow, A., Welihinda, A., Hayes, A., Radford, A., et al., 2024. Gpt-4o system card. arXiv:2410.21276 .
- [9] Kim, S., Xiao, R., Alaniz, S., Xian, Y., Akata, Z., 2025. Training-free uncertainty guidance for complex visual tasks with mllms. arXiv preprint arXiv:2510.00705 .
- [10] Lee, J., Choi, Y., Choi, H., Kim, H., Kim, S., 2025. A training-free, task-agnostic framework for enhancing mllm performance on high-resolution images. arXiv preprint arXiv:2507.10202 .
- [11] Li, B., Huang, W., Gao, Z., Wang, Y., Shen, Y., Lin, J., You, L., Shen, Y., Lin, S., Ouyang, W., et al., 2025a. Llava-radz: Can multimodal large language models effectively tackle zero-shot radiology recognition? arXiv preprint arXiv:2503.07487 .
- [12] Li, M., Chen, K., Bi, Z., Liu, M., Peng, B., Niu, Q., Liu, J., Wang, J., Zhang, S., Pan, X., et al., 2024a. Surveying the mllm landscape: A meta-review of current surveys. arXiv preprint arXiv:2409.18991 .
- [13] Li, Y., Du, Y., Zhou, K., Wang, J., Zhao, W.X., Wen, J.R., 2023. Evaluating object hallucination in large vision-language models. arXiv preprint arXiv:2305.10355 .
- [14] Li, Y., Liu, Z., Li, Z., Zhang, X., Xu, Z., Chen, X., Shi, H., Jiang, S., Wang, X., Wang, J., et al., 2025b. Perception, reason, think, and plan: A survey on large multimodal reasoning models. arXiv preprint arXiv:2505.04921 .
- [15] Li, Z., Yang, B., Liu, Q., Ma, Z., Zhang, S., Yang, J., Sun, Y., Liu, Y., Bai, X., 2024b. Monkey: Image resolution and text label are important things for large multi-modal models, in: proceedings of the IEEE/CVF conference on computer vision and pattern recognition, pp. 26763–26773.
- [16] Liu, H., Li, C., Li, Y., Li, B., Zhang, Y., Shen, S., Lee, Y.J., 2024. Llava-next: Improved reasoning, ocr, and world knowledge. URL: <https://llava-vl.github.io/blog/2024-01-30-llava-next/>.
- [17] Liu, H., Li, C., Wu, Q., Lee, Y.J., 2023. Visual instruction tuning. Advances in neural information processing systems 36, 34892–34916.
- [18] Neubeck, A., Van Gool, L., 2006. Efficient non-maximum suppression, in: 18th international conference on pattern recognition (ICPR'06), IEEE, pp. 850–855.
- [19] OpenAI, 2025. Thinking with images. <https://openai.com/index/thinking-with-images/>.
- [20] Schwenk, D., Khandelwal, A., Clark, C., Marino, K., Mottaghi, R., 2022. A-okvqa: A benchmark for visual question answering using world knowledge, in: European conference on computer vision, Springer, pp. 146–162.
- [21] Shen, H., Zhao, K., Zhao, T., Xu, R., Zhang, Z., Zhu, M., Yin, J., 2025. Zoomeye: Enhancing multimodal llms with human-like zooming capabilities through tree-based image exploration, in: Proceedings of the 2025 Conference on Empirical Methods in Natural Language Processing, pp. 6613–6629.
- [22] Wang, H., Su, A., Ren, W., Lin, F., Chen, W., 2025a. Pixel reasoner: Incentivizing pixel-space reasoning with curiosity-driven reinforcement learning. arXiv preprint arXiv:2505.15966 .
- [23] Wang, S., Liu, B., Gao, Z., Ma, L., Wang, X., Xie, Y., Tan, X., 2026. Explore with long-term memory: A benchmark and multimodal llm-based reinforcement learning framework for embodied exploration. arXiv preprint arXiv:2601.10744 .
- [24] Wang, W., Ding, L., Zeng, M., Zhou, X., Shen, L., Luo, Y., Yu, W., Tao, D., 2025b. Divide, conquer and combine: A training-free framework for high-resolution image perception in multimodal large language models, in: Proceedings of the AAAI Conference on Artificial Intelligence, pp. 7907–7915.
- [25] Wang, W., Gao, Z., Gu, L., Pu, H., Cui, L., Wei, X., Liu, Z., Jing, L., Ye, S., Shao, J., et al., 2025c. Internvl3.5: Advancing open-source multimodal models in versatility, reasoning, and efficiency. arXiv:2508.18265 .
- [26] Wei, J., Wang, X., Schuurmans, D., Bosma, M., Xia, F., Chi, E., Le, Q.V., Zhou, D., et al., 2022. Chain-of-thought prompting elicits reasoning in large language models. Advances in neural information processing systems 35, 24824–24837.
- [27] Wu, P., Xie, S., 2024. V?: Guided visual search as a core mechanism in multimodal llms, in: Proceedings of the IEEE/CVF Conference on Computer Vision and Pattern Recognition, pp. 13084–13094.
- [28] Xu, B., Lu, Y., 2025. Tecp: Token-entropy conformal prediction for llms. Mathematics 13, 3351.
- [29] Yaldiz, D.N., Bakman, Y.F., Buyukates, B., Tao, C., Ramakrishna, A., Dimitriadis, D., Zhao, J., Avestimehr, S., 2025. Do not design, learn:

A trainable scoring function for uncertainty estimation in generative llms, in: Findings of the Association for Computational Linguistics: NAACL 2025, pp. 691–713.

- [30] Zhang, J., Khayatkhoei, M., Chhikara, P., Ilievski, F., 2023. Towards perceiving small visual details in zero-shot visual question answering with multimodal llms. arXiv preprint arXiv:2310.16033 .
- [31] Zhang, J., Khayatkhoei, M., Chhikara, P., Ilievski, F., 2025a. Mllms know where to look: Training-free perception of small visual details with multimodal llms. arXiv preprint arXiv:2502.17422 .
- [32] Zhang, T., Shi, H., Wang, Y., Wang, H., He, X., Li, Z., Chen, H., Han, L., Xu, K., Zhang, H., et al., 2025b. Tokur: Token-level uncertainty estimation for large language model reasoning. arXiv preprint arXiv:2505.11737 .
- [33] Zheng, Z., Yang, M., Hong, J., Zhao, C., Xu, G., Yang, L., Shen, C., Yu, X., 2025. Deepeyes: Incentivizing "thinking with images" via reinforcement learning. arXiv:2505.14362 .
- [34] Zhu, D., Chen, J., Shen, X., Li, X., Elhoseiny, M., 2023. Minigpt-4: Enhancing vision-language understanding with advanced large language models. arXiv preprint arXiv:2304.10592 .